

The stress corrosion cracking (SCC) susceptibility of the dissimilar ASTM A36 Steels and 316L stainless steels welding in varied temperature of FeCl₂

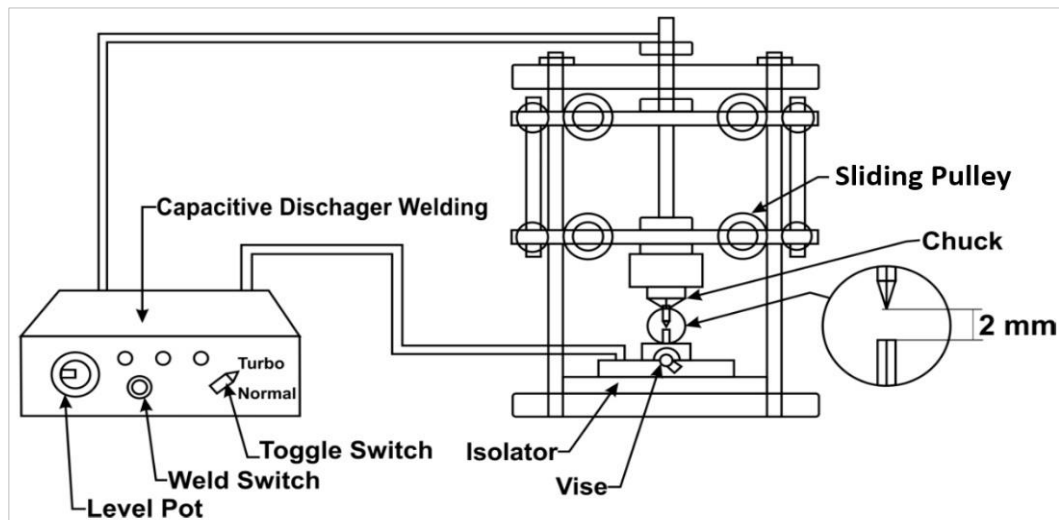
Djarot Bangun Darmadi^{1*}, Angga Saputra², Slamet Prasetyo Utomo¹, Marco Talice³

¹ Department of Mechanical Engineering, Universitas Brawijaya, Malang 65145, Indonesia

² Department of Mechanical Engineering, Politeknik Negeri Samarinda, Samarinda 75131, Indonesia

³ PMSQUARED Engineering S.r.l.s, 99 via Sydney Sonnino, Cagliari 09127, Italy

✉ b_darmadi_djarot@ub.ac.id



Highlights:

- A dissimilar welding joint was produced with controlled parameters using Capacitive Discharge Welding.
- Evaluate the joint in the elevated temperature of Stress Corrosion Cracking (SCC) load.
- Providing macrograph and SEM-EDS data to support the conclusion of the SCC test.

Article info

Submitted:
2025-02-08

Revised:
2025-06-02

Accepted:
2025-06-04



This work is licensed under a Creative Commons Attribution-NonCommercial 4.0 International License

Publisher

Universitas Muhammadiyah
Magelang

Abstract

Obtaining perfect dissimilar welding joints which are exposed to corrosive environments still a problem up to now. The ASTM A36 and 316L stainless steels dissimilar metals were joined by means of Capacitive Discharge Welding (CDW). The welding parameters such as distance between metals, pressure, applied energy, and surface parameter were kept constant. The FeCl₂ corrosive solution concentration also kept constant at 0.5M. The temperature of the solution was controlled at varied temperature, those are: 30 °C, 40 °C and 50 °C respectively. The resistance to the Stress Corrosion Cracking (SCC) load, was evaluated by time to fracture for certain dead tensile load and corrosive media. The SEM EDS data were retrieved to have deep insight of the SCC mechanism. The results show that, with 10 °C increasing temperature the SCC Threshold is decreased by 40% which are supported by the data of time to failure for certain load and also the SEM EDS.

Keywords: SCC susceptibility; SCC threshold; Dissimilar Joints; Capacitive discharge; Welding

1. Introduction

Considering the reliability of welding joints, it always becomes a concern for engineers, as it is almost impossible to provide a perfect joint. It will be more challenging when it is needed to join dissimilar metals. The recent issue of the welding is the resilience of the joint when exposed to

Stress Corrosion Cracking load, which is found that the joint will fail even when the applied load is far below the strength of the joint.

The application of welding was sped up during World War II when it was used to install plates in the Liberty hull. Since it was the early stage of applying welding massively, a lot of problems and failures existed, and many research studies were carried out afterward, up to the recent years. Kotecki and Moll noted that the excessive killing agent in the electrode core obstructs the formation of fine-grained ferrite, which in turn decreases the toughness of the joints [1]. While the addition of iron, beryllium, or chromium has been applied to the 70-30 CuNi alloys, it was proved that the alloys lose their strength at the heat-affected zone when welding is applied [2]. Olson [3] developed a method to predict the developed microstructure, especially the martensite start temperature of the weld joints for the austenitic steels with a high manganese content, which is devoted to obtaining optimum properties and service behavior. Kou and Le [4] investigated the effect of heat input and welding speed while Gas Tungsten Arc Welding is applied to aluminum alloys. The temperature in the weld pool was recorded, and the developed equiaxed grain in the welding was evaluated using optical and electron microscopes. The thermodynamic effect of heat input and welding speed was evaluated based on the experimentally measured G/R ratios, which both increase due to the welding speed. However, the increasing welding speed and heat input resolve the decreasing G/R ratio. From a thermodynamic point of view, this lower G/R ratio produces heterogeneous nucleation, which in turn refines the final produced grains. The welding parameters have also been investigated while the GTAW was applied to the high/low sulphur steels [5], [6]. Higher welding current and heat input do increase the penetration in high sulphur steels, but heat input has no effect in low sulphur steels even the current decreases the penetration. The penetration decreases for both high/low low-sulfur steels with higher welding speed and arch length. Adeyeye and Oyawale proposed what is called a mixture experiment, a statistical modelling tool, to overcome the time, labor, and intensive experimentation in developing welding flux when the traditional manner is used [7].

Not only for joining, welding may be applied for repairing. Pozo et al. [8] optimized the GMAW parameters when using it to repair the Pelton turbine blades. The optimization utilizes a genetic algorithm using the samples that use the controlled parameters. Those samples were then evaluated after experiencing a chemical attack and allowed observation of dilution, weld area, and penetration. The results show that the genetic algorithm provides good prediction with an error of less than 6%. Sonar et al. scrutinized the welding parameters of Constricted Arc – Tungsten Inert Gas Welding (CA-TIG) on tensile strength, weld bead, and microstructure of the resulting joints [9]. The CA-TIG was applied on AMS-5596 grade high-performance nickel-based material, which is also called Superalloy 718. The parameters that have significant effects on the developed microstructure are the main current (MC) and constricted arc traverse speed (CATS). They significantly affect the growth of dendrites, morphology, and % volume percentage of laves precipitates in the fusion zone (FZ) in which finally determines the tensile strength of the joint. The weld bead geometry is also significantly affected by both parameters (MC and CATS).

It is already known that corrosion has detrimental effects on a metal construction [10], [11], and after the blow up of pipelines in Argentina [12] and Winnipeg, Canada [13], the importance of considering SCC resiliencies in welding joints is emerged. Those blow-ups triggered an investigation of the failures in the weld joint due to the SCC phenomenon. Heat input is one of the important factors in the welding process [14], [15], [16]. The effect of Heat input on the SCC behaviors was studied by Anita *et al.* [17]. The intergranular stress corrosion cracking is formed while residual stress is developed in the TIG welding process of stainless steel 316 LN, which is called sensitization. The Cr₂₃C₆ precipitation while the Austenitic Stainless Steels are exposed to a temperature of 723 to 1123 K is the root cause of the sensitization [18]. Generally, the 7xxx series of aluminum alloy has lower SCC resistance compared to the 5xxx series. The 7xxx series may have good resistance to SCC in the longitudinal direction, but it is susceptible in the thickness direction. The existence of residual stresses even worsens the susceptibility of the 7xxx series [19]. Higher heat input or slower cooling rate reforms austenite during cooling and, in turn, degrades the corrosion resistance of welded duplex stainless steels significantly [20], [21]. The vulnerable microstructure in HAZ and the formation of residual stress when GTA welded joints of Super 304H austenitic stainless steel decrease the resistance to the SCC load [22], [23].

The data, such as slope of curve before transition (ISS), time to transition from secondary to tertiary regions (TSS), and time to fracture (TF), were obtained from the corrosion elongation curves. From the elongation curves, it can be concluded that the higher applied stress decreases the value of tss/tf, which indicates that the time to fail after the crack initiation is relatively longer,

and the ISS is increased, which means the crack initiates faster. Many failures of welded austenitic stainless steels, which are used in nuclear power plants, have been found in located at Heat Affected Zone (HAZ), especially when the SCC phenomenon emerges. The susceptibility of HAZ due to the microstructure change during the welding process [24], [25]. The important role of microstructure (type and size), especially in the direction of crack growth, has also been underlined by Darmadi *et al.* [26]. Kumar and Balasubramanian [27] applied autogenous GTAW on 304HCu Super Stainless Steel, in which the joint was exposed to boiling $MgCl_2$ solution afterward. The applied load stress was varied to 0.4, 0.6, 0.8, and 1.0 of yield stress of the base metal. Sepe *et al.* studied the SCC behavior of a welded S690Q HSS plate [28]. The welding process was carried out using Metal Inert Gas Welding. When the joint is exposed to the artificial seawater (pH = 4), its resistance to the SCC is decreased due to both anodic dissolution and hydrogen embrittlement mechanisms taking place.

The idea of Capacitive Discharge Welding (CDW) lies in the relatively slow storage of energy in a capacitor that is then released very rapidly, allowing high currents to flow in a very short time, making CDW increasingly attractive, particularly for dissimilar welding joints [29]. Ketzal *et al.* [30] evaluated joint development in CDW and demonstrated that metal vaporization occurs at the edges due to high current density, with the current density assumed to be even higher at the center of the projection because metal vapor has low electrical conductivity [30]. The quality of CDW joints, especially regarding stress corrosion cracking (SCC), can be improved by carefully designing the joint interface [31]. Despite such advancements, SCC remains a significant challenge, particularly in welded joints, as these inherently contain residual stresses and crack initiation sites, which, upon exposure to a corrosive environment, promote the emergence of SCC, a problem that becomes more severe in dissimilar metal joints. Therefore, this paper investigates the SCC behavior of CDW dissimilar metal joints in $FeCl_2$ solution, focusing on how variations in the temperature of the corrosive medium influence this phenomenon.

2. Materials and Methods

The dissimilar welded joints were obtained from the CDW apparatus using a special jig (shown in Figure 1) to obtain a constant welding condition. A detailed CDW process can be found in the previous article [31]. The constant parameters for the CDW process are: the distance between the specimen: 2mm, the pressure = 40N, the energy stored in the capacitor before welding is applied: 220 Joule. Bimetal CDW was applied to the joint of 316L stainless steel and ASTM A36 steel. To obtain good coalescence in the interface, the stainless steel was sharpened to 30° whilst the A36 steel was left flat. The composition and mechanical properties of both metals can be seen in Table 1 and Table 2.

After producing joints with comparable properties under controlled conditions, the specimens were subjected to stress corrosion cracking (SCC) tests, where the only variable changed was the temperature of the corrosive 0.5 M $FeCl_2$ solution, set at $30^\circ C$, $40^\circ C$, and $50^\circ C$. A schematic of the SCC test apparatus is shown in Figure 2, featuring a closed-loop temperature control to maintain consistent solution temperatures during testing. Different load levels were applied to identify the SCC threshold, with the time to fracture recorded as the key measurement for each combination of load and temperature. Each test condition was repeated three times, and the average time to fracture was used as the representative value. To gain deeper insights into SCC mechanisms under various temperatures, SEM-EDS analyses were performed on the fracture surfaces.

Table 1.
Element composition

ASTM A36 Steel						
Fe	C	Al	S	Cr	Si	Ni
Bal.	0.148	0.001	0.02	0.046	0.0015	0.092
P	Cr	Mn	W			
0.008	0.103	0.555	0.04			
316L Stainless Steel						
Fe	C	Al	S	Cr	Si	Ni
Bal.	0.025	-	0.01	16.38	0.41	9.60
P	Cr	Mn	W	Mo	Cu	Co
0.04	17.9	1.60	-	3.15	0.51	0.28

Table 2.
Material properties

	Melting Point ($^\circ C$)	UTS (MPa)	Hardness BHN	Density (g/cm^3)
ASTM A36 Steel	1450	440	120	7.87
316L Stainless Steel	2540	515	149	8.00

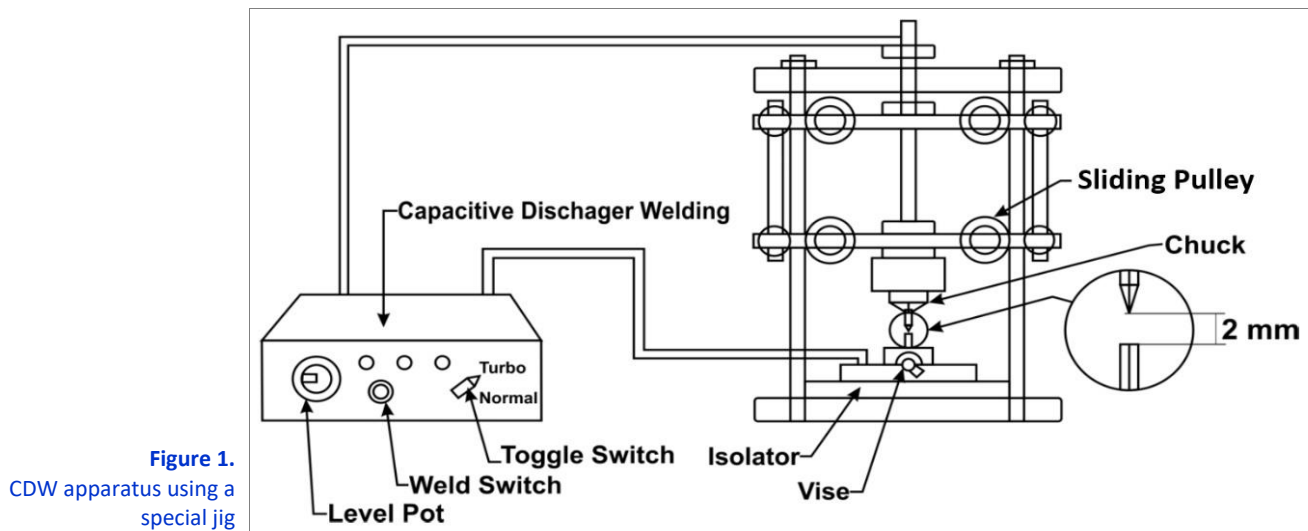


Figure 1.
CDW apparatus using a
special jig

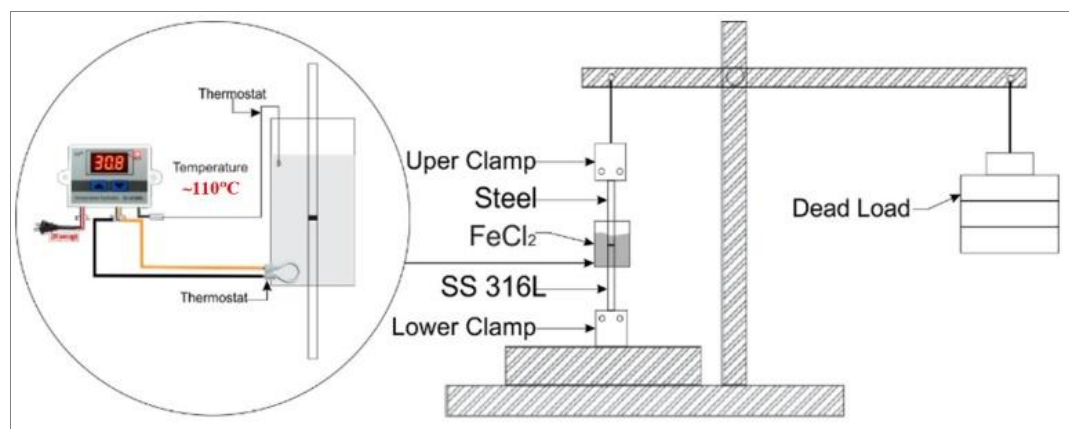


Figure 2.
SCC test apparatus

3. Results and Discussion

The SCC resilience of the joints is obtained by evaluating the time to fail when the joints are exposed to the corrosive solution with varied temperature while the dead load is applied. The dead load varies from 5 to 45 kg with 5 kg increments, which coincides with 107.87, 245.74, 326.61, 431.87, 539.35, 647.22, 755.09, 862.95, and 970.83 MPa, respectively. The temperature of the corrosive solution was 30 °C, 40 °C, and 50 °C. For each variation, three data points on time to fail are retrieved, and the results can be seen in [Table 3](#). When a 970.83 MPa load was applied, the joints suddenly failed in all temperature variations of the corrosive solution since the load is above the mean of ultimate strength of the joints (around 862.96 MPa). When the load which close to the ultimate strength was applied, at 30 °C the joints stood only for around 7 minutes (average) before they failed, while when exposed to 40 °C and 50 °C, the joints failed instantaneously.

To obtain a clearer understanding of [Table 3](#), it is presented in a graph as shown in [Figure 3](#). The lines are drawn from the mean that the blue, yellow, and red lines represent the 30 °C, 40 °C, and 50 °C of corrosive solution temperature, respectively. To interpret [Figure 3](#), we can evaluate the graph for an equal time to fail (same abscissa) or for similar load (identical ordinate). If evaluation is applied for time to fail equal to 450 minutes, for example, and when the joint is exposed to 30 °C, 40 °C, and 50 °C of corrosive solution, it corresponds to the load equal to 365 MPa, 252 MPa, and 150 MPa subsequently. This means with higher temperature, the joint will stand an equal duration for a lower load. Simpler understanding can be obtained by evaluating the equal load (same ordinate). If evaluation is applied to the time to fail when 450 MPa is applied to the joint while exposed to a varied temperature of the environment, for the 30 °C, 40 °C, and 50 °C of corrosive solution, the times to fail are around 70, 14,0, and 270 minutes, respectively. It can be said that an increasing temperature of a corrosive environment decreases the time to fail while the load (in MPa) is equal. This method of interpretation can be tested at all times to fail or all applied loads, and will come to the same conclusion.

When the curve's tangent line close to horizontal, it is considered it reaches to the stress corrosion threshold that when the load is below the threshold the joint will not fail due to the SCC

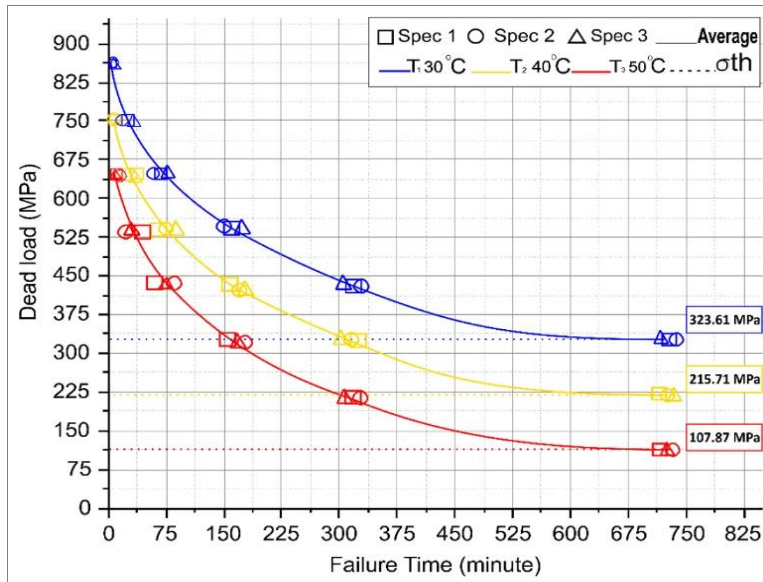


Figure 3. SCC test results

mechanism. In practice, when the load was under SCC threshold the joint was not broke until 5 hours and we stop the SCC test to save the time. From the Figure 3, it can be said that the SCC thresholds are 323.61 MPa, 215.71 MPa and 107.87 MPa when the joint is immersed in the 30 °C, 40 °C and 50 °C of corrosive environment that the SCC threshold decreases with the temperature.

Table 3. The SCC data

Load (Kg)	Stress (MPa)	T1 (30 °C)		T2 (40 °C)		T3 (50 °C)	
		Time To Fail (Minute)	Mean (Minute)	Time To Fail (Minute)	Mean (Minute)	Time To Fail (Minute)	Mean (Minute)
5	107.87	2500	2517.66	1630	1535.33	726	725.33
		2521		1625		723	
		2531		1653		727	
10	215.74	1631	1659.66	724	724.33	316	318.33
		1695		728		319	
		1653		721		320	
15	323.61	726	722.66	310	315.33	168	169.33
		723		320		165	
		719		316		175	
20	431.87	310	316.66	179	170.66	78	75.33
		315		168		73	
		325		165		75	
25	539.35	175	170.33	75	72.33	28	27.33
		165		69		25	
		168		73		29	
30	647.22	66	68.33	24	25.33	10	10.66
		68		25		14	
		71		27		8	
35	755.09	23	25.33	6	5	2	1.66
		27		5		2	
		27		4		1	
40	862.96	5	6.66	0	0.00	0	0.00
		9		0		0	
		6		0		0	
45	970.83	0	0.00	0	0.00	0	0.00
		0		0		0	
		0		0		0	

The evaluated broken surface while the joint is exposed to the SCC environment at the load close to the SCC threshold can be seen in Figure 4. The surface was obtained by exposing the joint to a varied temperature of corrosive environment, i.e., 30 °C, 40 °C, and 50 °C. Thus, there are areas where the corrosion phenomenon dominates, and catastrophic areas where the load is the main factor of SCC. From Figure 4, it can be seen that the corrosion area will be wider due to the temperature, which means that with this temperature, the corrosion becomes more detrimental, which confirms the conclusions which is obtained from Figure 3. To ensure the area that is considered as SCC area is correct, the EDS test was applied to the selected areas (shown as a red square), and the results are shown in Table 4. The corrosion products of ASTM A36 and 316L stainless steels are Ferrous and Chromium oxides. The Chromium oxides is produced by the 316L stainless steel, which contains a significant amount of Chrome (16.38%). It can be seen from Table 4; the product of corrosion is higher due to the temperature of corrosive media. Thus, not only the

area but also the intensity of the corrosion product, especially in the inspected “point” is also higher. This phenomenon proved that higher temperatures are more severe to the joint from the SCC point of view.

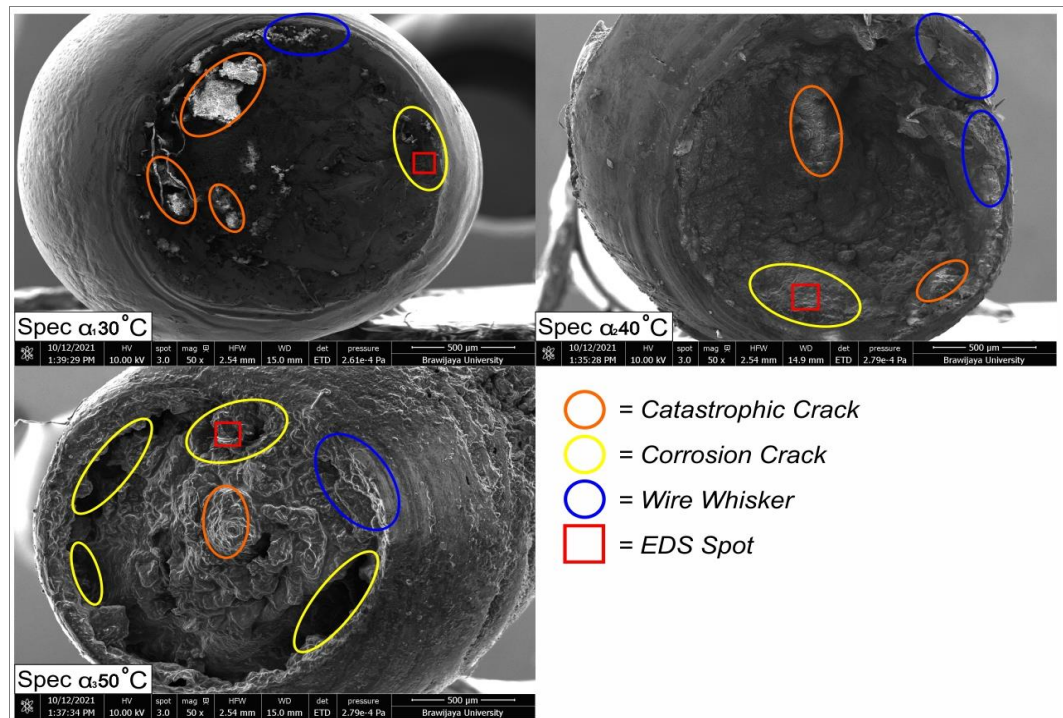


Figure 4.
The morphology of fracture surfaces when exposed to SCC load

Table 4.
The EDS results of the selected area in the fracture surfaces

Specimen	Element's composition (%)					
	C	Cr	Fe	Cl	O	Si
30 °C	92.46	-	6.73	0.71	-	0.10
40 °C	67.58	-	10.56	1.89	19.34	0.55
50 °C	31.05	9.03	44.23	0.52	9.01	0.44

In **Figure 5** to **Figure 7** are scrutinized the EDS results of the fracture surface when immersed in the 30 °C, 40 °C and 50 °C of the FeCl₂ respectively. The (a) pictures show the surface when magnified 100x, (b) show the enlarged EDS spot which is dominated by a corrosion, while (c), (e) and (f) are EDS layered image for the carbon, oxygen and Fe elements and (d) shows the chemical elements mapping in a graph. The corrosion in the SCC phenomenon is initiated with tiny voids or oxidation holes which grew in the fracture area. The corrosion in SCC is more severe due to the tensile load. The O element is resulted by oxidation while Fe and C is from the base metal. The Cr element is the dominant alloying element from the 316L stainless steels.

In **Figure 5** is shown a crack which grows in a dense fracture surface with less corrosion cavities which cannot be observed. When exposed to 40 °C FeCl₂. Evaluating **Figure 6**, there is a pitch which indicates the existence of oxidation. The high oxide indicates the severity of corrosion. Oxidation significantly impact failure in a dissimilar welding joint, leading to oxide scale development and spallation due to thermal expansion mismatch between oxide scale and underlying metals [32], [33]. The oxides with FeCl₂ produce gases that represent redox reaction. As can be seen in **Table 4**, the oxygen content generally increases for the elevated temperature of corrosive solution which represents the increasing severity. The Chrome content start to exist when the corrosive solution at 50 °C. Basically the corrosion in the metals follows electrochemical mechanism. Electrochemical corrosion is the shifting product of combined galvanic cells that cause microscopic short-circuits on metals of alloys surface which in contact with electrolytic solution [34], [35]. In **Figure 7d**, it is shown the scatter EDS disperse of Fe, C, O and Cr elements from the fracture surface of the joint when exposed to 50 °C FeCl₂ corrosive solution which indicates the high concentration due to the elevated temperature. This is confirmed by a paper by Sanchez *et al.* [36] that the temperature of corrosive solution causes a tin film layer eroded faster due to cathode reaction. Increasing the temperature by 10 °C accelerates the corrosion rate by 2.5 times of the normal temperature [37], [38], [39]. When the temperature of alloys on dissimilar metal welds changed, the ductile-to-brittle transition temperatures changed. This, in turn, changed how the cracks stopped spreading and how they stopped growing [40], [41]. Increasing the temperature contributes to the number of

active corrosion centers in the metal surfaces and finally increase the corrosion rate [42], [43]. Ju *et al.* [44] reported the effect of high temperature corrosive environment that accelerates corrosion and the crack growth rate in the SCC phenomenon will also be increased. Following the Arrhenius law in basic chemistry, when an acid (such as chloride - HCl) is solved in water will produce H⁺ ion. When the temperature increases, the concentration of acid increases and the electrochemical reaction increases thus increases the corrosion rate especially the dissolution of anodic metals. All of this previous research confirms the detrimental effect of the temperature and in this research is shown that increasing the FeCl₂ corrosive solution by 10 °C decreases the SCC threshold by around 40% as shown in Figure 3.

Figure 5.
Evaluated SEM-EDS morphology of the T30 °C fracture surface specimen in Figure 4:
a) Evaluated area of the fracture surface;
b) SEM;
c) EDS – Carbon Mapping;
d) EDS Spectra Material Xxx;
e) EDS Oxygen Mapping
f) EDS Fe Mapping

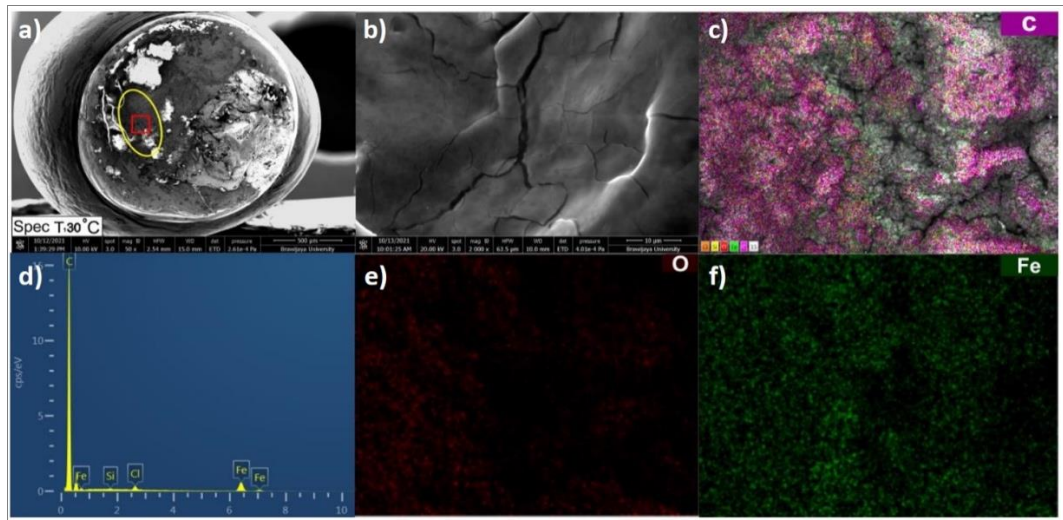


Figure 6.
Evaluated SEM-EDS morphology of the T40 °C fracture surface specimen in Figure 4:
a) Evaluated area of the fracture surface;
b) SEM;
c) EDS – Carbon Mapping;
d) EDS Spectra Material Xxx;
e) EDS Oxygen Mapping;
f) EDS Fe Mapping

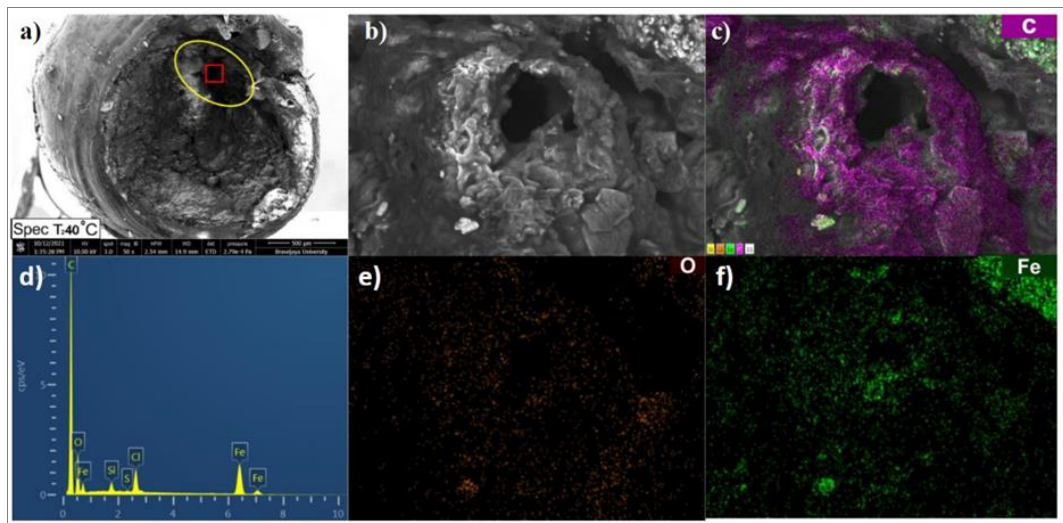
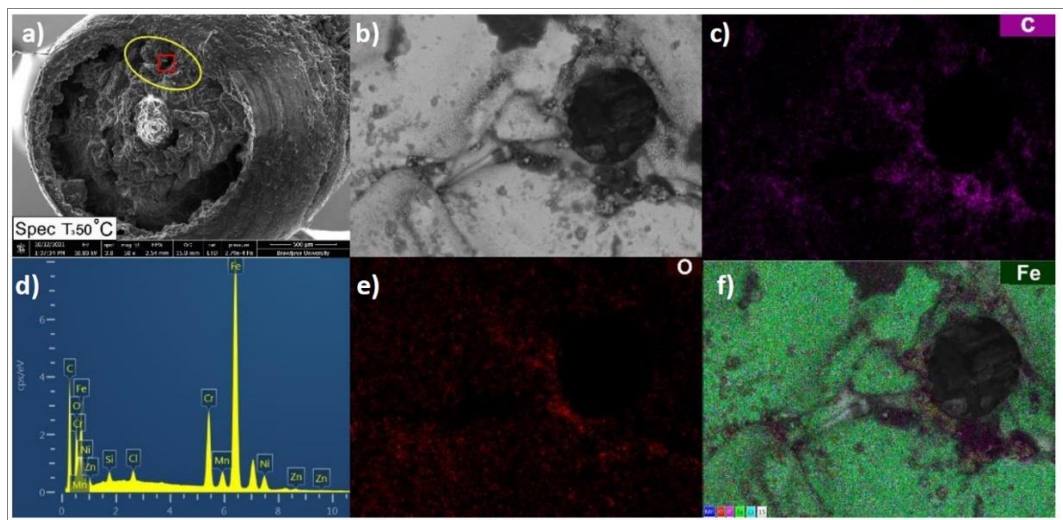


Figure 7.
Evaluated SEM-EDS morphology of the T50 °C fracture surface specimen in Figure 4:
a) Evaluated area of the fracture surface;
b) SEM;
c) EDS – Carbon Mapping;
d) EDS Spectra Material Xxx;
e) EDS Oxygen Mapping;
f) EDS Fe Mapping



To gain a better understanding how the SCC takes places in **Figure 8** are shown the fracture surfaces when the joint immersed in the 30 °C FeCl₂ solution for 75, 170, 300, 700 and 1600 minutes while the 15 kg dead load which equal to 323.61 MPa is applied in SCC mode followed by an ultimate load to obtain the fracture surfaces. Analogue to **Figure 4**, the surface comprises of SCC and catastrophic areas which are obtained from SCC and ultimate loads respectively. Although those fracture surfaces are not obtained from a single specimen which is impossible, but how the SCC develops in the joint can be depicted quit well. As it is shown by **Figure 8**, the SCC area increases with time. The elements composition which is obtained from EDS test ensure that the area which are determined as the SCC area contains the elements of corrosion’s product and tabulated in **Table 5**. The Chromium element exist from the early time since the load is higher compare to the load in the previous sets and it content tends to increase with time. Remembering the EDS spots is obtained from different specimen, a little discrepancy of the Chromium content at 75, 170 and 300 minutes is understandable. The oxygen always increases due to the longer SCC load time which is consistent since the Oxygen is the main indication of corrosion severity.

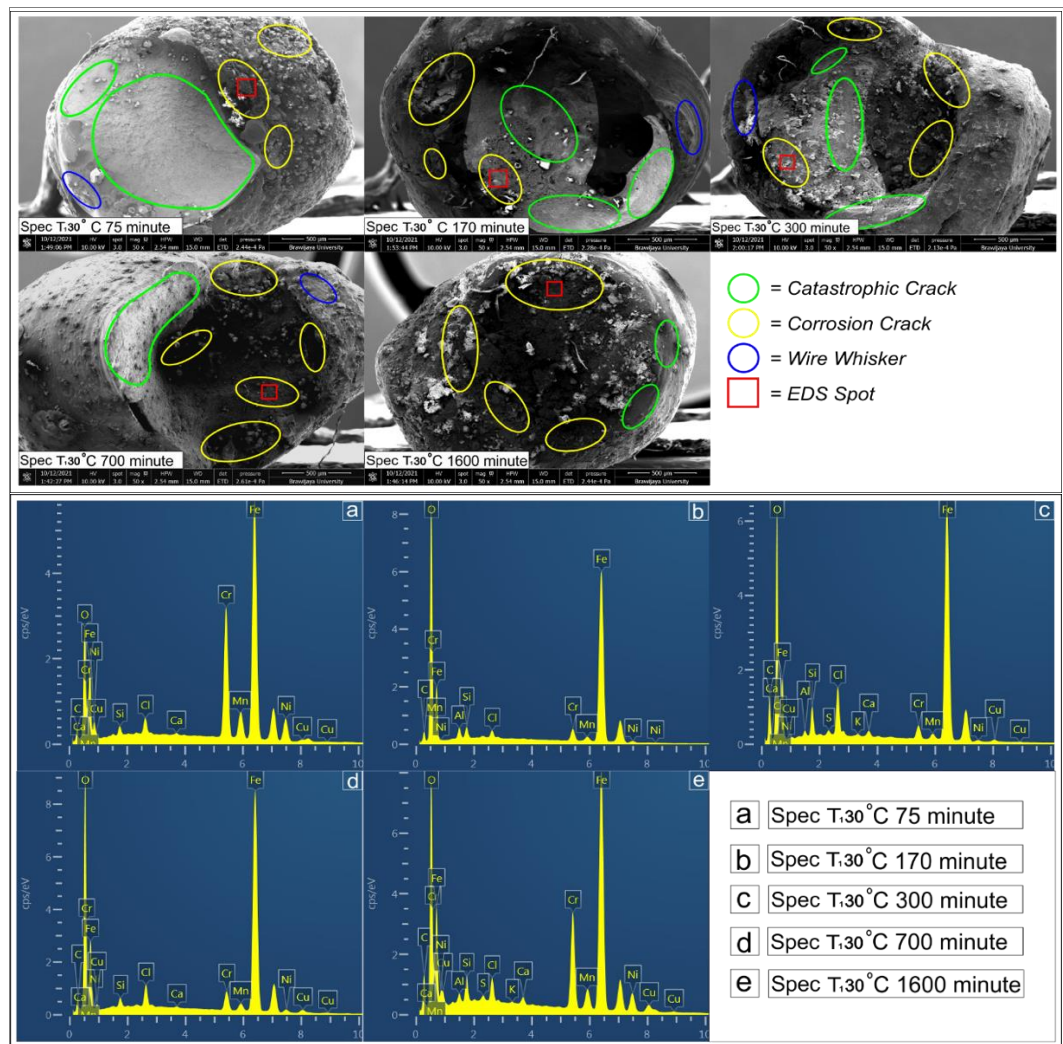


Figure 8.
The SCC development by longer immersed time

Table 5.
Chemical composition for increasing dipping time

Exposing Time	Elements						
	C	Cr	Fe	Cl	O	Si	Ni
75 min	6.82	2.78	55.55	1.48	11.24	0.58	1.23
170 min	5.22	1.48	54.59	2.37	22.19	1.30	0.47
300 min	6.00	2.26	52.59	0.96	27.74	0.56	0.89
700 min	13.83	10.50	44.79	0.66	28.88	0.86	7.89
1600 min	19.45	17.77	41.42	13.83	33.75	1.06	5.00

4. Conclusion

The SCC test indicates that temperature is a key factor influencing the SCC phenomenon. When considering a specific load, higher temperatures reduce the specimen's lifetime under SCC

conditions. Likewise, for a given duration, increasing temperature lowers the maximum load the specimen can withstand without failure. Temperature reduces the time to collapse of the dissimilar joint. The SCC threshold for the joint at 30 °C, 40 °C, and 50 °C is 323.61 MPa, 215.71 MPa, and 323.61 MPa, respectively. This indicates that as temperature increases, the maximum load that can be sustained without triggering the SCC phenomenon decreases. The SEM EDS results also confirm the results. Although the SEM EDS results are taken from different specimens, the development of the corroded area can be well described.

Acknowledgments

I would like to express gratitude to Brawijaya University, especially BPPM FTUB to all facility and finance support to carry out this research.

Authors' Declaration

Authors' contributions and responsibilities - The authors made substantial contributions to the conception and design of the study. The authors took responsibility for data analysis, interpretation and discussion of results. The authors read and approved the final manuscript.

Funding – BPPM Faculty of Engineering, Brawijaya University.

Availability of data and materials - All data is available from the authors.

Competing interests - The authors declare no competing interests.

Additional information – No additional information from the authors.

References

- [1] D. J. Kotechi and R. A. Moll, "A Toughness Study of Steel Weld Metal from Self-Shielded Flux-Cored Electrodes – Part I," *Welding Journal*, vol. 4, pp. 157s – 165s, 1970.
- [2] P. W. Holsberg, "Weldability Studies of Modified 70-30 CuNi Alloys," *Welding Journal*, vol. 12, pp. 554s–558s, 1970.
- [3] D. L. Olson, "Prediction of Austenitic Weld Metal Microstructure and Properties," *Welding Journal*, vol. 10, pp. 281s–295s, 1985.
- [4] S. Kou and Y. Le, "Welding parameters and the grain structure of weld metal — A thermodynamic consideration," *Metallurgical Transactions A*, vol. 19, no. 4, pp. 1075–1082, Apr. 1988, doi: 10.1007/BF02628392.
- [5] A. A. Shirali and K. C. Mills, "The Effect of Welding Parameters on Penetration in GTA Welds," *Welding Journal*, vol. 7, pp. 347s–353s, 1993.
- [6] Z. Afriansyah, M. Ashof, and A. Naimah, "Comparison of SMAW and GTAW Welding Properties," *Mechanics Exploration and Material Innovation*, vol. 1, no. 2, pp. 48–53, Apr. 2024, doi: 10.21776/ub.memi.2024.001.02.2.
- [7] A. D. Adeyeye and F. A. Oyawale, "Mixture experiments and their applications in welding flux design," *Journal of the Brazilian Society of Mechanical Sciences and Engineering*, vol. 30, no. 4, pp. 319–326, Dec. 2008, doi: 10.1590/S1678-58782008000400008.
- [8] L. Pérez Pozo, F. Olivares Z, and O. Durán A, "Optimization of welding parameters using a genetic algorithm: A robotic arm–assisted implementation for recovery of Pelton turbine blades," *Advances in Mechanical Engineering*, vol. 7, no. 11, Nov. 2015, doi: 10.1177/1687814015617669.
- [9] T. Sonar, V. Balasubramanian, S. Malarvizhi, T. Venkateswaran, and D. Sivakumar, "Effect of welding parameters on microstructure and tensile properties of CA-TIG welded AMS-5596 grade thin high temperature alloy sheets for gas turbine engine applications," *Advances in Industrial and Manufacturing Engineering*, vol. 2, p. 100035, May 2021, doi: 10.1016/j.aime.2021.100035.
- [10] S. N. Fitriani, P. H. Setyarini, and V. Y. Risonarta, "The Influence of Homogenization on Corrosion Rate of Zinc as Sacrificial Anode for API 5L X65 Steel," *International Journal of Mechanical Engineering Technologies and Applications*, vol. 1, no. 1, p. 7, Jan. 2020, doi: 10.21776/mechta.2020.001.01.2.

- [11] D. H. Akbar, P. Purnami, and S. P. Budio, "Influence of Surface Roughness and Paint Coating on Corrosion Rate," *International Journal of Mechanical Engineering Technologies and Applications*, vol. 1, no. 1, p. 15, Jan. 2020, doi: 10.21776/mechta.2020.001.01.3.
- [12] C. Manfredi and J. . Otegui, "Failures by SCC in buried pipelines," *Engineering Failure Analysis*, vol. 9, no. 5, pp. 495–509, Oct. 2002, doi: 10.1016/S1350-6307(01)00032-2.
- [13] J. Wang and A. Atrens, "Microstructure and grain boundary microanalysis of X70 pipeline steel," *Journal of Materials Science*, vol. 38, pp. 323–330, 2003, doi: 10.1023/A:1021169700779.
- [14] Djarot B. Darmadi, Lingga P. Setiawan, and Shahrudin Mahzan, "Evaluating the GMAW Joint with a Constant Heat Input," *Journal of Advanced Research in Fluid Mechanics and Thermal Sciences*, vol. 54, no. 2 SE-Articles, pp. 142–149, Mar. 2024, [Online]. Available: https://semarakilmu.com.my/journals/index.php/fluid_mechanics_thermal_sciences/article/view/3036
- [15] E. P. Budiana, S. G. H. Hapsari, E. R. I. Mahmoud, and T. Triyono, "Temperature and material flow in one-step double-acting friction stir welding process of aluminum alloy: Modeling and experimental," *Mechanical Engineering for Society and Industry*, vol. 5, no. 1, pp. 145–157, Apr. 2025, doi: 10.31603/mesi.12987.
- [16] S. Sukarman et al., "Optimization of Tensile-Shear Strength in the Dissimilar Joint of Zn-Coated Steel and Low Carbon Steel," *Automotive Experiences*, vol. 3, no. 3, pp. 115–125, Oct. 2020, doi: 10.31603/ae.v3i3.4053.
- [17] T. Anita, H. Shaikh, H. S. Khatak, and G. Amarendra, "Effect of Heat Input on the Stress Corrosion Cracking Behavior of Weld Metal of Nitrogen-Added AISI Type 316 Stainless Steel," *Corrosion*, vol. 60, no. 9, pp. 873–880, Sep. 2004, doi: 10.5006/1.3287869.
- [18] D. H. Kumar and a. S. Reddy, "Study of Mechanical Behavior in Austenitic Stainless Steel 316 Ln Welded Joints," *International Journal of Mechanical Engineering and Robotics Research*, vol. 2, no. 1, pp. 1–22, 2013.
- [19] D. W. Rathod, "A Review on challenges and opportunities in wire arc additive manufacturing of aluminium alloys: Specific context of 7xxx series alloys," *Mechanical Engineering for Society and Industry*, vol. 5, no. 1, 2025, doi: 10.31603/mesi.12711.
- [20] K. Chan and S. Tjong, "Effect of Secondary Phase Precipitation on the Corrosion Behavior of Duplex Stainless Steels," *Materials*, vol. 7, no. 7, pp. 5268–5304, Jul. 2014, doi: 10.3390/ma7075268.
- [21] J. Andrean, A. Harmayanti, A. Wahjudi, and A. Syamlan, "Analysis of The Corrosion Inhibition Efficacy of Camellia Sinensis Extract on Aluminium 6061 Alloys using Artificial Neural Network (ANN)," *Mechanics Exploration and Material Innovation*, vol. 1, no. 2, pp. 67–74, Apr. 2024, doi: 10.21776/ub.memi.2024.001.02.5.
- [22] M. Vinoth Kumar, V. Balasubramanian, S. Rajakumar, and S. K. Albert, "Stress corrosion cracking behaviour of gas tungsten arc welded super austenitic stainless steel joints," *Defence Technology*, vol. 11, no. 3, pp. 282–291, Sep. 2015, doi: 10.1016/j.dt.2015.05.009.
- [23] D. F. Fitriyana et al., "Effect of sandblasting on the characterization of 95MXC coating layer on 304 stainless steel prepared by the twin wire arc spray (TWAS) coating method," *Mechanical Engineering for Society and Industry*, vol. 4, no. 2, pp. 142–155, Nov. 2024, doi: 10.31603/mesi.10898.
- [24] H.-L. Ming et al., "Microstructure, Residual Strain and Stress Corrosion Cracking Behavior in 316L Heat-Affected Zone," *Acta Metallurgica Sinica (English Letters)*, vol. 29, no. 9, pp. 848–858, Sep. 2016, doi: 10.1007/s40195-016-0461-7.
- [25] T. S. Amosun, S. O. Hammed, A. M. G. De Lima, and I. Habibi, "Effect of quenching media on mechanical properties of welded mild steel plate," *Mechanical Engineering for Society and Industry*, vol. 3, no. 1, pp. 4–11, Sep. 2022, doi: 10.31603/mesi.7121.
- [26] D. B. Darmadi, N. A. Sugiarto, and F. Gapsari, "Stress Corrosion Cracking at ASTM A36 Plate with Varied Grain Orientation," *International Review of Mechanical Engineering (IREME)*, vol. 12, no. 12, p. 987, Dec. 2018, doi: 10.15866/ireme.v12i12.16532.
- [27] M. V. Kumar and V. Balasubramanian, "Hot tensile properties and constant load stress corrosion cracking test data of autogenous weld joints of super 304H Cu stainless steel in boiling MgCl₂ solution," *Data in Brief*, vol. 18, pp. 102–110, Jun. 2018, doi:

- 10.1016/j.dib.2018.03.002.
- [28] R. Sepe, F. Bollino, F. Caiazzo, and F. Berto, "Stress corrosion cracking behavior of welding joint of high strength steel," *IOP Conference Series: Materials Science and Engineering*, vol. 1038, no. 1, p. 012055, Feb. 2021, doi: 10.1088/1757-899X/1038/1/012055.
- [29] N. Scotchmer, "The use of capacitor discharge welding is on the rise," *Welding Journal*, vol. 94, no. 2, pp. 32–36, 2015.
- [30] M.-M. Ketznel, M. Hertel, J. Zschetsche, and U. Füssel, "Heat development of the contact area during capacitor discharge welding," *Welding in the World*, vol. 63, no. 5, pp. 1195–1203, Sep. 2019, doi: 10.1007/s40194-019-00744-x.
- [31] D. B. Djarot, F. Gapsari, O. B. Lobo, and F. M. Simanjuntak, "Stress Corrosion Cracking Threshold for Dissimilar Capacitive Discharge Welding Joint with Varied Surface Geometry," *Applied Sciences*, vol. 10, no. 6, p. 2180, Mar. 2020, doi: 10.3390/app10062180.
- [32] X. Li et al., "Oxidation damage and interfacial failure of dissimilar metal welds containing ferritic heat resistant steels," *Journal of Iron and Steel Research International*, vol. 28, no. 11, pp. 1439–1450, Nov. 2021, doi: 10.1007/s42243-021-00586-2.
- [33] J. Cui and D. Wang, "An experimental and numerical investigation on ultimate strength of stiffened plates with opening and perforation corrosion," *Ocean Engineering*, vol. 205, p. 107282, Jun. 2020, doi: 10.1016/j.oceaneng.2020.107282.
- [34] P. Marcus, I. Frateur, and V. Maurice, "Évolution des méthodes et outils de recherche sur la corrosion," *Matériaux & Techniques*, vol. 99, no. 1, pp. 13–33, Jan. 2011, doi: 10.1051/mattech/2010113.
- [35] T. F. Cui, D. X. Liu, P. A. Shi, J. J. Liu, Y. H. Yi, and H. L. Zhou, "Effect of NaCl concentration, pH value and tensile stress on the galvanic corrosion behavior of 5050 aluminum alloy," *Materials and Corrosion*, vol. 67, no. 1, pp. 72–83, Jan. 2016, doi: 10.1002/maco.201408189.
- [36] S. Sanchez et al., "Powder Bed Fusion of nickel-based superalloys: A review," *International Journal of Machine Tools and Manufacture*, vol. 165, p. 103729, Jun. 2021, doi: 10.1016/j.ijmachtools.2021.103729.
- [37] P. Refait, A.-M. Grolleau, M. Jeannin, E. François, and R. Sabot, "Corrosion of mild steel at the seawater/sediments interface: Mechanisms and kinetics," *Corrosion Science*, vol. 130, pp. 76–84, Jan. 2018, doi: 10.1016/j.corsci.2017.10.016.
- [38] A. Barasa, A. Wahjudi, R. R. Pratama, and W. Kriswardhana, "Adding ZnO to Cellulose/ZnO Nanocomposites Coated A36 Steel Increases The Corrosion Rate," *Mechanics Exploration and Material Innovation*, vol. 1, no. 3, pp. 82–87, 2024, doi: 10.21776/ub.memi.2024.001.03.2.
- [39] B. Amelia, M. N. Ilman, and N. A. Triwibowo, "Minimizing distortion in flux cored arc welding of A36 steel by preheating and its effect on weld mechanical properties," in *The 6th BIS-STE 2024 in conjunction with The 2nd INTERCONNECTS 2024*, 2025. doi: 10.31603/biseeng.209.
- [40] S. Lindqvist, Z. Que, P. Nevasmaa, and N. Hytönen, "The effect of thermal aging on fracture properties of a narrow-gap Alloy 52 dissimilar metal weld," *Engineering Fracture Mechanics*, vol. 281, p. 109056, Mar. 2023, doi: 10.1016/j.engfracmech.2023.109056.
- [41] Margono, M. Kozin, D. Setiadi, H. K. Hassan, and R. Lakshminarasimhan, "Development of Titanium Nitride-Based Coatings for Wear Resistant Materials: A Review," *Mechanics Exploration and Material Innovation*, vol. 1, no. 3, 2024, doi: 10.21776/ub.memi.2024.001.03.5.
- [42] V. Konovalova, "The effect of temperature on the corrosion rate of iron-carbon alloys," *Materials Today: Proceedings*, vol. 38, pp. 1326–1329, 2021, doi: 10.1016/j.matpr.2020.08.094.
- [43] P. Astuti, A. D. Puspitasari, A. Zulkarnain, A. C. Fajar, and A. Y. Purnama, "Corrosion evaluation of patch repair material using seawater mixed mortar," in *The 6th BIS-STE 2024 in conjunction with The 2nd INTERCONNECTS 2024*, 2025. doi: 10.31603/biseeng.340.
- [44] H. Ju, Y.-F. Yang, Y.-F. Liu, S.-F. Liu, J.-Z. Duan, and Y. Li, "Mapping the Galvanic Corrosion of Three Metals Coupled with a Wire Beam Electrode: The Influence of Temperature and Relative Geometrical Position," *Materials*, vol. 11, no. 3, p. 357, Feb. 2018, doi: 10.3390/ma11030357.